The role of platinum on the NO_x storage and desorption behavior of ceria: An online FT-IR study combined with *in situ* Raman and UV-Vis spectroscopy

*Anastasia Filtschew[†], Pablo Beato[‡], Søren B. Rasmussen[‡], and Christian Hess[†]**

[†] Eduard-Zintl-Institut für Anorganische und Physikalische Chemie, Technische Universität Darmstadt, Alarich-Weiss-Straße 8, 64287 Darmstadt, Germany

[‡] Haldor Topsøe A/S, Haldor Topsøes Allé 1, DK-2800 Kgs. Lyngby, Denmark

*e-mail: christian.hess@tu-darmstadt.de

Keywords:

Ceria, Pt, NO, NO_x storage, PNA, oxygen activation, mechanism, Raman, UV-Vis

Urheberrechtlich geschützt / In Copyright: https://rightsstatements.org/page/InC/1.0/

Abstract

The role of platinum on the room temperature NO_x storage mechanism and the NO_x desorption behavior of ceria was investigated by combining online FT-IR gas-phase analysis with *in situ* Raman and UV-vis spectroscopy. The type of pretreatment, leading to the presence of different platinum states (Pt^0, mixed Pt^0/Pt^{2+}), is shown to have a major effect on the NO_x storage and desorption properties. Upon loading of ceria with platinum (1wt%), NO_x storage capacities decrease except for reductively pretreated Pt/CeO_2, enabling new reaction pathways via activation of gas-phase oxygen. In the absence of oxygen, NO is reduced by metallic platinum leading to N_2O and N_2 formation. *In situ* Raman spectra provide mechanistic information, by monitoring changes in ceria surface and subsurface oxygen, as well as PtO_x during NO_x storage. In the presence of gas-phase oxygen, NO_x storage is related to the consumption of (sub)surface oxygen and PtO_x, and proposed to involve NO_2 or $[NO+O_2]$ intermediates reacting with surface oxygen. The NO_x desorption behavior is shown to be strongly related to the stored NO_x species. Oxidative pretreatment of ceria resulted in the largest amount of stored nitrates, consistent NO_x being mostly desorbed at elevated temperatures, i.e., within 300-500°C. Reductive pretreatment and/or addition of platinum significantly increased the fraction of stored nitrite, thereby shifting the main NO_x desorption temperature to values <300°C. Storage and subsequent desorption of NO_x in PtO_x/CeO_2 was associated with PtO_x reduction and reoxidation, as monitored by *in situ* UV-Vis and Raman spectra. By detailed analysis we were able to elucidate the influence of platinum on NO_x storage/desorption and demonstrate the participation of different platinum states in room temperature NO_x storage, with each platinum state opening a distinct new reaction pathway.

Introduction

Exhaust emissions caused by industry and automobiles are one of the most serious environmental problems leading to negative effects on atmosphere, global ecosystem and human health. The goal is to reduce exhaust emissions, e.g. by establishing regulations for the emission of pollutants like nitrogen oxides (NO_x). To reduce NO_x emissions different technologies have been discussed in literature, such as direct decomposition of NO to N_2 and O_2,[1, 2] selective catalytic reduction (SCR) of NO_x,[3-5] NO_x storage reduction (NSR) or lean NO_x traps catalysts (LNT),[6-11] and low-temperature NO_x adsorbers (LTNA) or passive NO_x adsorber (PNA)[12-16]. The NSR/LNT catalyst and LTNA/PNA systems have in common that initially NO_x is stored in a NO_x storage material. As NO_x storage materials Al_2O_3,[17, 18] barium oxide,[19, 20] ceria containing materials,[10-12, 14, 21-26] as well as mixtures of these[8, 11, 27-31] have been discussed.

A major challenge in NO_x reduction is the NO_x treatment at low temperatures (<200°C). To this end, LTNA/PNA systems are of great interest, which allow NO_x storage at low temperatures (<200°C) and their release at higher temperatures, followed by a treatment by another deNO_x system such as a SCR catalyst.[6-16] A benefit of ceria is that it can store NO_x already at room temperature.[10, 12] There are a number of publications investigating the NO_x storage behavior of ceria containing materials at temperatures >80°C,[6-9, 13, 14, 21, 23, 32-36] but only a few cover lower temperatures.[10, 12, 37, 38] Furthermore, while it is established that precious metals like platinum or palladium can promote the NO_x storage in ceria containing materials at temperatures >100°C,[14, 21] little is known about the role of platinum during NO_x storage at lower temperatures.

To elaborate the role of platinum during NO_x storage, the state of platinum under *in situ* conditions is of great interest. To detect platinum in different states *in situ* or quasi *in situ*, various techniques are available, such as Raman spectroscopy,[39-41] UV-vis spectroscopy,[42-45] near-ambient

pressure X-ray photoelectron spectroscopy (NAP-XPS),[46] and X-ray absorption spectroscopy (XAS),[47, 48] Unlike NAP-XPS, XA spectroscopy can be routinely applied at ambient pressure and high pressures,[49] as can be Raman and UV-Vis spectroscopy. Raman spectroscopy allows PtO_x species to be observed but metallic platinum is not accessible.[50] In principle, UV-Vis spectroscopy has the potential to detect both metallic and oxidized platinum,[44] and it has therefore been applied to the characterization of platinum-loaded samples,[42-45] without using it under *in situ* conditions. Limitations may arise for larger metallic platinum particles, leading to strong absorption within the range 400-1000 nm, and hence decreasing the sensitivity to detect PtO_x. However, this limitation can be overcome by a combination of UV-vis and Raman spectroscopy, enabling the detection of both metallic and oxidized platinum, even under *in situ* conditions. Consequently, observations made during NO_x adsorption/desorption can be directly correlated with the platinum state present under the respective reaction conditions.

A promotional effect of PtO_x during NO_x storage at 200°C was already observed by Luo *et al.*.[23] For reductively pretreated Pt/CeO_2 at >200°C it is assumed that NO_x storage is promoted by NO oxidation catalyzed by metallic Pt^0, since more NO_2 than NO can be stored in ceria.[7, 12, 14, 51] However, at lower temperatures, the role of platinum state for NO_x storage is still unknown. In this context, it is also of interest whether the presence of gas-phase oxygen has an influence on NO_x storage. Li *et al.* assumed that metallic platinum on ceria can activate molecular oxygen already at room temperature.[52] In turn, such a low-temperature oxygen activation by platinum would be expected to influence the NO_x storage capacity.

In this study, we elucidate the role of platinum on the NO_x storage in ceria from a fundamental point of view, by performing NO_x storage experiments in ceria and platinum loaded ceria at room temperature. Using oxidative or reductive pretreatment prior to NO_x storage different

platinum states were generated. Comparison of NO_x storage with and without oxygen allows us to gain insight into the influence of oxygen on NO_x storage. We employ a combination of *in situ* Raman and *in situ* UV-vis spectroscopy to characterize the state of ceria and platinum, while the exhaust is monitored by quantitative FT-IR gas-phase analysis to calculate the NO_x storage capacity and NO_x desorption efficiency. Sample degradation by laser radiation is avoided by use of a fluidized-bed approach.[53] To explore the role of platinum and the platinum state during NO_x desorption we analyzed the temperature-dependent desorption behavior O_2/N_2 after one hour of NO_x storage.

Experimental

Material synthesis

The ceria sample was synthesized by a twofold calcination of cerium(III) nitrate hexahydrate (Sigma Aldrich, 99.999% trace metal basis) at 600°C (6°C/min) for 12 h. The 1 wt% Pt/CeO_2 sample was prepared by incipient wetness impregnation of an aqueous solution of tetraammineplatinum(II) nitrate (ROTH®METIC, Roth) onto the synthesized ceria sample. Then the Pt-loaded ceria sample was dried at 85°C overnight and calcined at 500°C (6°C/min) for 2 h. For the investigations 200-300 μm sieve fractions were used.

Sample characterization

The samples were characterized by N_2 adsorption-desorption, X-ray diffraction, and X-ray photoelectron spectroscopy (XPS). Nitrogen adsorption-desorption experiments were performed on a NOVA 3000e (Quantachrome). Prior to the measurements the samples were evacuated for 24

h at 150°C. The specific surface area was determined by the Brunauer-Emmett-Teller (BET) method.

X-ray diffraction patterns were recorded on an X-ray powder diffractometer (StadiP, Stoe & Cie GmbH) with a Mythen 1K (Dectris) detector. The measurements were performed in transmission geometry with a Cu Kα1 radiation (λ=1.540598 Å) and a Ge[111] monochromator. To estimate the crystal sizes of the samples the Scherrer equation with K=0.89 (spheric crystals) was used.

XP spectra were recorded on a SSX 100 ESCA spectrometer (Surface Science Laboratories Inc.) under high vacuum conditions, using monochromatic Al Kα radiation. The spot size was 0.25×1.00 mm². To minimize charging effects an electron flood gun with an energy of 0.5 eV was used. XP spectra were recorded at room temperature with a step size of 0.1 eV and analyzed using the software Casa XPS. Binding energies were calibrated by shifting the C 1s peak to 285 eV.

Experimental setup

The samples were investigated by Raman and UV-vis spectroscopy using a commercial CCR1000 catalyst cell from Linkam Scientific Instruments (see Fig. 1). The ceramic sample holder was loaded with about 130 mg of CeO_2 or Pt/CeO_2 sample on a ceramic fiber fleece. To avoid sample damage by laser radiation, a fluidized bed was used by placing a membrane pump in the downstream, as described previously.[53] The pressure oscillations of the membrane pump were controlled by a regulating transformer, allowing to adjust the mixing speed.

For a quantification of stored NO_x amount, the outlet gas was connected to a FT-IR spectrometer (Bruker Tensor 27, DLaTGS (deuterated and L-alanine-doped triglycine sulfate)) equipped with a low volume gas cell (25 mL, Axiom, LFT). The gas cell was heated to 125°C to

avoid water condensation. FT-IR spectra were measured with a resolution of 4 cm^{-1} and an aperture of 6 mm. The quantification of NO_x in the outlet gas and as a consequence the stored NO_x amount in the sample was calculated by calibration curves. The NO_x storage capacity was determined by subtracting the breakthrough curves of the loaded catalyst cell from the empty catalyst cell.

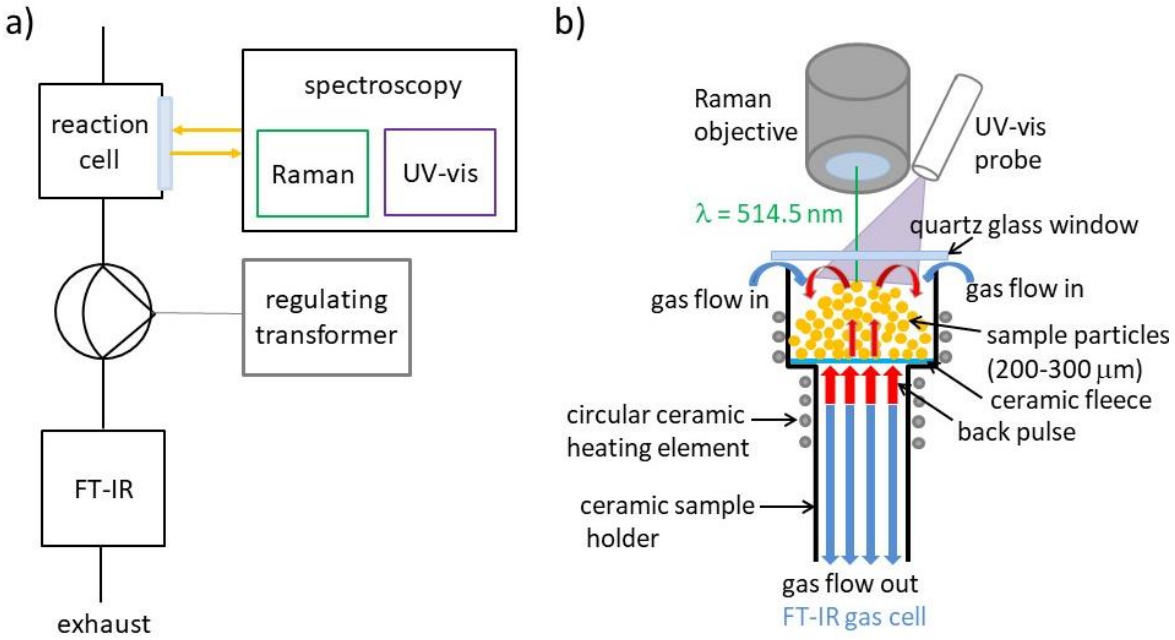

Fig. 1 a) Schematic drawing of the experimental setup. b) Schematic drawing of the sample holder of the CCR1000 catalyst cell with arrows indicating the gas flow directions. For details see text.

Raman spectra were recorded in a backscattering geometry using an argon-ion (514.5 nm, Melles Griot) or Nd:YAG (532 nm, Cobolt) laser. NO_x storage experiments with oxygen were investigated at 514.5 nm laser excitation, while for NO_x storage without oxygen a laser wavelength of 532 nm was employed. Please note that after normalization to the F_{2g} mode of ceria (~464 cm^{-1}), spectra of both laser wavelength coincide very well, except for the worse signal-to-noise ratio at 532 nm excitation and background effects (see Fig. S1). The laser power was adjusted to 2.3

mW at the location of the sample. The backscattered light was collected by a transmission spectrometer (Kaiser Optical), equipped with a charge-coupled device (CCD) detector and calibrated with a standard argon lamp. The resolution of the spectrometer was 5 cm^{-1}, but the wavelength stability was better than 0.5 cm^{-1}. For the fitting of Raman signals, Voigt functions with (instrumental) Gaussian linewidth of 6 cm^{-1} were used. In case of the Ce-O-signal related changes after NO_x storage we first calculated difference spectra, based on the spectrum prior NO_x exposure, and then applied the fitting analysis.

UV-Vis spectra were measured on an AvaSpec-ULS2048 spectrometer (Avantes), employing a halogen and a deuterium lamp (AvaLight-DHS, Avantes) for excitation. The UV-vis fiber was tilted by 30° with respect to the Raman objective. To avoid interference effects, Raman and UV-vis spectra were recorded alternately.

Initially, all samples were pretreated either oxidatively or reductively. During oxidative pretreatment the sample was heated in 50 ml/min 20% O_2/N_2 to 400°C for 1 h (heating rate: 20°C/min). For reductive treatment the sample was heated in 50 ml/min 20% O_2/N_2 to 400°C for 30 min (heating rate: 20°C/min). Afterwards, 50 ml/min N_2 were flowed through the sample to remove oxygen and subsequently switched to 50 ml/min 7.5% H_2/Ar at 400°C for 30 min. Then the sample was cooled to 30°C in 50 ml/min N_2 (cooling rate: 20°C/min). At 30°C the feed was switched to 50 ml/min 20% O_2/N_2 for 10 min.

NO_x storage was performed either with or without the presence of oxygen in the feed. For NO_x storage with oxygen, 1000 ppm NO/N_2 were mixed with 20% O_2/N_2 resulting in a gas reaction mixture of 500 ppm NO/20% O_2/N_2. For NO_x storage without oxygen, 50 ml/min N_2 were flowed through the sample for 30 min prior to NO_x storage to remove oxygen from the catalyst cell. Then 1000 ppm NO/N_2 were mixed with nitrogen to achieve a gas reaction mixture of 500 ppm NO/N_2.

Results and discussion

Sample characterization

Prior to any pretreatment and NO_x storage, both samples were characterized by X-ray diffraction and nitrogen adsorption-desorption experiments. Both samples have a similar BET surface area of 64.5 m^2/g for bare ceria and 72.2 m^2/g for platinum-loaded ceria. The crystal size of the CeO_2 sample was about 25-30 nm, while ceria in the loaded sample had a crystal size of about 15-20 nm, coinciding with the larger surface area. We cannot rule out that the observed deviations in crystal size and surface area result from different sample charges, as new ceria was synthesized for the loaded sample. Based on XPS experiments on the platinum-loaded sample the platinum content was determined as 0.24 at% (see Table S1), which is equivalent to 1.14 wt% Pt on the surface. Detailed XPS analysis revealed that 53.4% of the platinum were in a metallic state (Pt^0) and 46.6% in an oxidized (Pt^{2+}) state (see Table 1).

Table 1 Platinum state of the Pt/CeO_2 sample after respective treatment as determined by XPS analysis.

Sample	Pt^0 [%]	Pt^{2+} [%]
Pt/CeO_2, as synthesized	53.4	46.6
Pt/CeO_2, ox.	42.1	57.9
Pt/CeO_2, red.	100	0

Influence of pretreatment

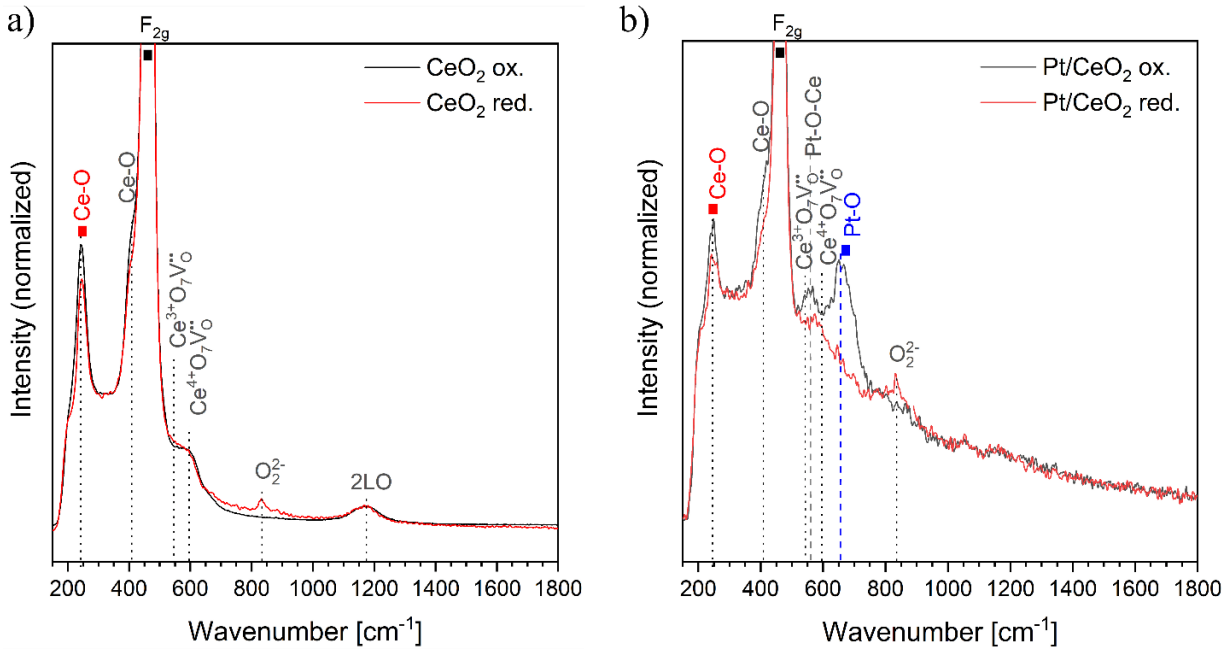

Fig. 2 Raman spectra recorded at 30°C of oxidatively (black) and reductively (red) pretreated a) CeO_2 and b) Pt/CeO_2. All spectra were normalized to the F_{2g} mode. To allow an enlarged view of the other signals, the high intensity of the F_{2g} mode at around 464 cm^{-1} was cut off.

Prior to NO_x storage, samples were characterized after oxidative and reductive pretreatment. Fig. 2 shows Raman spectra of CeO_2 and Pt/CeO_2 within the range 150-1800 cm^{-1}, characterized by features at 244, ~410, ~464, 550, and 595 cm^{-1}. The signals at 244 and ~410 cm^{-1} are assigned to the longitudinal and transversal stretching modes of the $CeO_2(111)$ surface and will be denoted here as Ce-O.[54] The most intense signal at ~464 cm^{-1} originates from the F_{2g} mode of ceria,[54, 55] while the signals at 550 and 595 cm^{-1} are attributed to a $Ce^{4+}O_7V_O^{\bullet\bullet}$ and $Ce^{3+}O_7V_O^{\bullet\bullet}$ coordination cube, respectively[54]. For oxidatively and reductively pretreated ceria an additional signal at 1164 cm^{-1} was observed and ascribed to the 2LO overtone of ceria.[55] The 2LO overtone was barely

visible in the Pt/CeO_2 spectra because of a poorer signal-to-noise ratio, caused by the strong absorption of the laser beam by platinum (see Fig. 3).

After reductive pretreatment the ceria sample showed an additional signal at 832 cm^{-1} assigned to the stretching vibration of peroxide originating from adsorption of molecular oxygen on surface oxygen vacancies.[56, 57] Besides, the Ce-O signal at 244 cm^{-1} of reductively pretreated ceria had a lower intensity than that of oxidatively pretreated ceria (see Table 2), indicating reduction of the ceria surface. However, since the F_{2g} position of the reductively pretreated ceria was at the same position as after an oxidative pretreatment, the subsurface of ceria was not reduced.

Table 2 F_{2g} positions and Ce-O signal area after oxidative or reductive pretreatment of CeO_2 and Pt/CeO_2.

Sample	**F_{2g} position [cm^{-1}]**	**Ce-O area (244 cm^{-1})**
CeO_2 ox.	464.6 (±0.1)	0.076 (±0.001)
CeO_2 red.	464.6 (±0.1)	0.056 (±0.002)
Pt/CeO_2 ox.	464.2 (±0.1)	0.072 (±0.004)
Pt/CeO_2 red.	464.0 (±0.1)	0.043 (±0.006)

Oxidatively pretreated Pt/CeO_2 showed two additional signals at 560 and 660 cm^{-1}, assigned to a Pt-O-Ce and Pt-O vibration of finely dispersed PtO_x, respectively.[41, 58] As shown above, 42.1% of platinum was present in as Pt^0 and 57.9% was oxidized (Pt^{2+}) (see Table 1), consistent with the observed PtO_x Raman signals. Therefore, compared to the as synthesized

Pt/CeO_2 sample, some of the metallic platinum was oxidized to PtO_x during the oxidative pretreatment. Additionally, in comparison to bare ceria, the F_{2g} mode was shifted to 464.2 cm^{-1} and the Ce-O area (244 cm^{-1}) decreased to 0.072 (see Table 2), indicating a reduction of the ceria subsurface and surface caused by strong metal support interaction (SMSI) between ceria and platinum,[40, 59, 60]

After reductive pretreatment of Pt/CeO_2 only very weak Raman signals of Pt-O-Ce and Pt-O were observed, indicating a reduction of PtO_x. Using XPS analysis only metallic platinum was detected on the surface (see Table 1). Furthermore, the intensity of both Ce-O signals (244 and 410 cm^{-1}) decreased and the F_{2g} mode shifted to 464.0 cm^{-1} (see Table 2). Thus, compared to the bare ceria sample, ceria in the reductively pretreated Pt/CeO_2 was reduced at the surface and subsurface, caused by hydrogen spillover from Pt to ceria.[41, 61] A reduction of the ceria surface was also verified by peroxide formation on surface oxygen vacancies (see Fig. 2).[56, 57]

In addition to Raman spectra, UV-vis spectra were measured after oxidative and reductive pretreatment of CeO_2 and Pt/CeO_2 (see Fig. 3). The signals at ~250 and 330 nm originate from O 2p(filled) → Ce 4f(empty) transitions and f → d transitions, respectively.[62, 63] After reductive pretreatment bare ceria showed a broad absorption within the range 500-1000 nm. This broad absorption is assigned to charge transfer from Ce^{3+} to Ce^{4+}, indicating ceria reduction.[63, 64]

When ceria is loaded with platinum new absorption signals are observed within the region 420-1000 nm. After oxidative pretreatment, a broad absorption feature extending over the range 420-700 nm is observed, which originates from PtO_x particles.[44, 45] Since a correlation between the absorption at 500 nm and the Raman intensity of the 660 cm^{-1} signal was found, the assignment of the broad UV-Vis signal to finely dispersed PtO_x was verified (see Fig. S2). Furthermore, broad absorption was observed within the region 420-1000 nm, which is attributed to metallic platinum

particles.[45] Hence, after oxidative pretreatment probably both finely dispersed PtO_x particles and metallic platinum particles were present on Pt/CeO_2, consistent with the XPS results (see Table 1). After reductive pretreatment, the Pt/CeO_2 sample showed only featureless broad absorption extending over the range 420-1000 nm, originating from larger metallic platinum particles.[45] Consequently, the reduced Pt loaded ceria sample consisted mainly of metallic platinum on ceria, as already observed by XPS analysis (see Table 1).

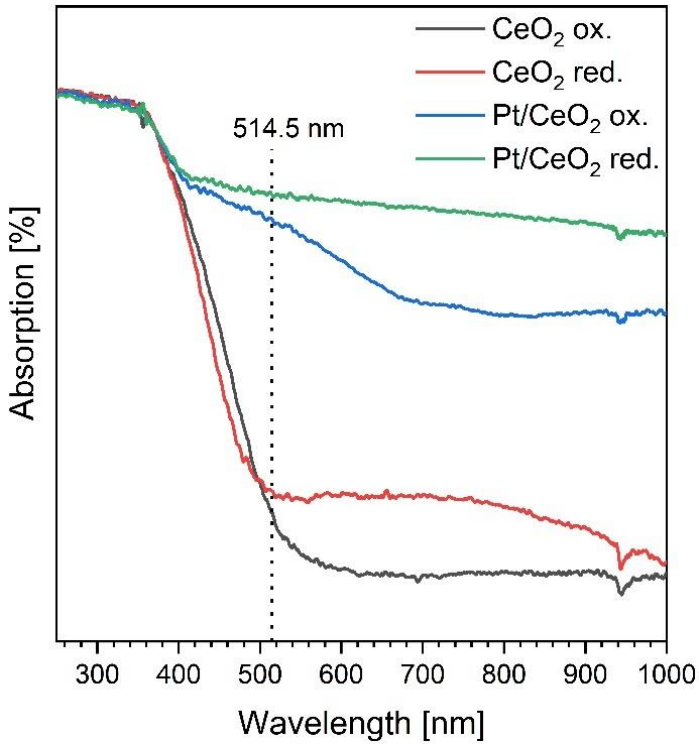

Fig. 3 UV-vis spectra of CeO_2 and Pt/CeO_2 after oxidative and reductive pretreatment.

NO_x storage capacity

Fig. 4 summarizes the NO_x storage capacities after one hour of NO_x storage with and without oxygen for the pretreated CeO_2 and Pt/CeO_2 samples. Apparently, the NO_x storage capacity is dependent on the type of pretreatment and on the presence of oxygen. In fact, already small

amounts of residual oxygen in the catalyst cell had a strong impact on the NO_x storage capacity (not shown). Therefore, to enable an investigation of NO_x storage without the presence of oxygen, it was crucial to remove oxygen by flushing the catalyst cell for 30 min with nitrogen.

Overall, the oxidatively pretreated ceria sample showed the best performance during NO_x storage with oxygen. In the absence of oxygen, the NO_x storage capacity dropped from 0.25 mmol/g to 0.11 mmol/g, indicating a participation of gas-phase oxygen in the NO_x storage mechanism. A similar capacity decrease was observed for reductively pretreated ceria, which was exposed to NO in the presence of oxygen. For NO_x storage in reductively pretreated ceria without oxygen, the lowest NO_x storage capacity of all samples was observed.

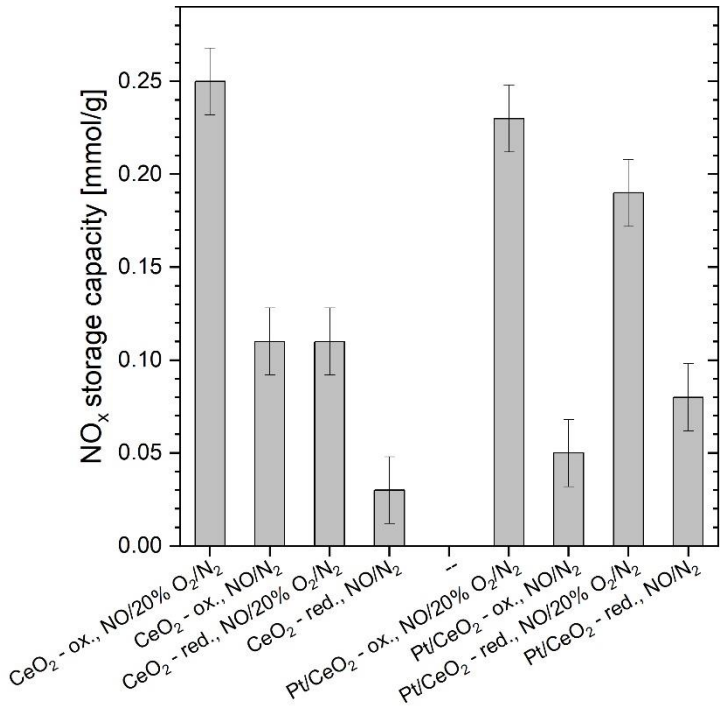

Fig. 4 NO_x storage capacity after one hour of NO_x storage at 30°C with and without oxygen in CeO_2 and Pt/CeO_2.

Upon loading with platinum, the oxidatively pretreated sample had a lower NO_x storage capacity than bare ceria, indicating that addition of platinum to ceria had an adverse effect on the storage properties. However, if the platinum-loaded ceria sample was pretreated reductively, the NO_x storage capacity increased compared to reductively pretreated ceria, thus indicating a beneficial effect of the presence of platinum. Nevertheless, NO_x storage capacities of reductively pretreated Pt/CeO_2 were still lower than those after NO_x storage with oxygen in oxidatively pretreated Pt/CeO_2 and CeO_2. On the other hand, for reductively pretreated Pt/CeO_2, an increase in NO_x storage capacity was detected indicating an activation of NO on platinum (see Fig. 4).

As for bare ceria the absence of oxygen had a strong impact on NO_x storage in Pt/CeO_2. In fact, the NO_x storage capacities decreased by more than a half of that observed in the presence of oxygen. The last column of Table 3 gives a summary of the NO_x storage capacities obtained in this study.

NO_x storage without oxygen in bare ceria

In the following, the NO_x storage data will be related to spectroscopic findings. To this end, Table 3 lists the observed F_{2g} shifts and Ce-O area changes from Raman spectra, and the corresponding NO_x storage capacities. As discussed previously, the observed F_{2g} shifts to lower wavenumbers can be attributed to an increase in the number of subsurface oxygen vacancies, i.e., a decrease in the concentration of subsurface oxygen.[12,54] When the NO_x storage experiments in ceria in the presence and absence of oxygen are compared, it is conspicuous that the Ce-O area change and F_{2g} shift are significantly smaller during the NO_x storage without oxygen. Therefore, gas-phase oxygen must play a crucial role in NO_x storage. If oxygen is present in the gas phase, NO was partly oxidized to NO_2 because of the thermodynamic equilibrium (see Fig. S3). Furthermore, it is

possible that a [NO+O_2] complex was formed,[65] eventually supported by the activation of gas-phase oxygen through ceria. Therefore, it is assumed, that mainly NO_2 and a possibly formed [NO+O_2] complex can react with surface oxygen of CeO_2(111), while NO does not interact or interacts only weakly with the CeO_2(111) surface, indicating that NO adsorbs on other adsorption sites than NO_2. As a result, notably lower NO_x storage capacities during NO_x storage in the absence of oxygen are obtained.

Table 3 F_{2g} shift, Ce-O area change (at 244 cm^{-1}), and NO_x storage capacity after one hour of NO_x storage at 30°C with and without oxygen. *The exact Ce-O area change could not be determined, since during reaction, simultaneously to the consumption of surface oxygen, new surface oxygen sites were generated leading to an intermediate increase of the Ce-O area (see Fig. S4).

Experiment	F_{2g} shift [cm^{-1}]	Ce-O area change [a. u.]	NO_x storage capacity [mmol/g]
CeO_2 ox. - NO/20% O_2/N_2	-1.0 (±0.1)	< -0.039 (±0.001)*	0.25 (±0.02)
CeO_2 ox. - NO/N_2	-0.2 (±0.1)	-0.015 (±0.002)	0.11 (±0.02)
CeO_2 red. - NO/20% O_2/N_2	-0.8 (±0.1)	-0.030 (±0.002)	0.11 (±0.02)
CeO_2 red. - NO/N_2	-0.0 (±0.1)	-0.002 (±0.003)	0.03 (±0.02)
Pt/CeO_2 ox. - NO/20% O_2/N_2	-0.5 (±0.1)	-0.025 (±0.004)	0.23 (±0.02)
Pt/CeO_2 ox. - NO/N_2	-0.2 (±0.1)	-	0.05 (±0.02)
Pt/CeO_2 red. - NO/20% O_2/N_2	-0.7 (±0.1)	-0.012 (±0.005)	0.19 (±0.02)
Pt/CeO_2 red. - NO/N_2	-0.6 (±0.1)	-	0.08 (±0.02)

DFT calculations have revealed that NO is preferentially adsorbed on surface oxygen vacancies and interacts only weakly with a fully oxidized ceria surface.[66-68] On oxygen vacancies NO^- species are formed, which can interact with neighboring surface oxygen. As a result, nitrite may be formed, which can migrate on the ceria surface. However, nitrite can dissociate back to NO^-.[68] If two NO adsorb on two neighboring surface oxygen vacancies or a nitrite species migrates to another adsorbed NO, the two NO^- are reduced to N_2 and the ceria surface is reoxidized.[66-68]

If NO was stored without oxygen in reductively pretreated ceria, NO is likely to adsorb on oxygen vacancies. Furthermore, eventually a reoxidation of the ceria surface with the formation of N_2 is expected. However, in the literature, a decomposition of NO to N_2 and O_2 over ceria was only observed at 673 K but not at low temperatures.[2] Therefore, it is rather assumed, that NO occupies surface oxygen vacancies forming nitrite without further migration on the ceria surface. Also, it cannot be excluded that NO was stored on surface sites different from the surface oxygen sites detected by Raman spectroscopy and oxygen vacancies. To this end, based on DFT calculations by Mihaylov *et al.*, NO adsorption could take place on edges of the ceria surface.[35]

NO_x storage in the absence of oxygen in oxidatively pretreated ceria resulted in a higher NO_x storage capacity compared to reductively pretreated ceria. This is against expectation, since reductively pretreated ceria had a higher amount of oxygen vacancies and therefore stronger adsorption sites for NO.[66-68] However, in oxidatively pretreated ceria still a noticeable amount of surface oxygen was consumed during the NO_x storage (see Table 3). Therefore, it is assumed, that even after 30 min of nitrogen flushing there was still adsorbed oxygen in the reaction cell or activated oxygen on the ceria surface, leading to the formation of NO_2 or $[NO+O_2]$ complexes and

subsequent reaction with surface oxygen. As a result, new oxygen vacancies may be formed, which could then adsorb NO followed by N_2 formation and reoxidation of the ceria surface, as described above.

In a previous study it was shown that in the presence of gas-phase oxygen the NO_x storage capacity was dependent on the amount of consumed surface oxygen, i.e., the decrease in Ce-O area.[12] However, in case of NO_x storage without oxygen in oxidatively pretreated ceria, the amount of consumed surface oxygen was too low to explain the higher NO_x storage capacity, since for NO_x storage with oxygen in reductively pretreated ceria more surface oxygen was consumed for the same amount of stored NO_x (see Table 3). Therefore, NO must have been adsorbed also on sites different from Ce-O and oxygen vacancy sites such as edges of the ceria surface.[35]

NO_x storage with oxygen in pure ceria

In the presence of oxygen, the value of the NO_x storage capacity, the Ce-O area decrease and the F_{2g} shift were significantly higher (see Table 3). According to our previous work NO_x storage with oxygen is strongly dependent on the number of available surface oxygen sites (Ce-O) and subsurface oxygen (F_{2g} shift).[12] Extending these findings, the results of this work indicate that a significant consumption of surface and subsurface oxygen occurs only in the presence of gas-phase oxygen, and is accompanied by the formation of NO_2 and probably formation of $[NO+O_2]$ complexes. It is assumed that NO_x storage in the presence of oxygen is strongly dominated by the reaction of these two species with surface oxygen, while direct NO adsorption plays a minor part. Consequently, compared to oxidative pretreatment, reductive pretreatment resulted in a lower NO_x storage capacity, since a lower amount of surface oxygen was available (see Fig. 2 and Table 2).

NO_x storage without oxygen in Pt/CeO_2

Depending on the type of pretreatment, the supported platinum was present in different states, leading to different influences on the NO_x storage, as described in the following. After reductive pretreatment, predominantly metallic platinum (see Table 1) and a higher concentration of oxygen vacancies compared to bare ceria was observed, as deduced from the lower Ce-O area and the F_{2g} redshift (see Table 2).

Haneda *et al.* investigated the NO decomposition over prereduced Pt/CeO_2 at room temperature, 473 K, and 673 K.[2] By employing mass spectrometry, the formation of 29.3 mmol/g N_2 and 5.9 mmol/g N_2O was observed at room temperature, while the ceria surface was reoxidized by the formed oxygen atoms. Since in our experiments in the initial 10 min of NO_x storage N_2O was also detected (see Fig. 5), we can confirm an activation and reduction of NO to N_2O and N_2 at 303 K. Furthermore, it is expected that during NO decomposition surface O_2 was formed, besides reoxidation of the ceria surface. The formed oxygen may react with NO to NO_2 and/or $[NO+O_2]$ complexes, followed by storage with the aid of Ce-O sites. As a consequence of surface oxygen consumption, oxygen from the subsurface diffuses to the surface,[12] explaining the relative high F_{2g} redshift during NO_x storage without oxygen compared to pure ceria and oxidatively pretreated Pt/CeO_2 (see Table 3). Therefore, in reductively pretreated Pt/CeO_2, NO was decomposed and stored via the formation of NO_2 and/or $[NO+O_2]$ complexes, resulting in a higher NO_x storage capacity compared to oxidatively pretreated Pt/CeO_2.

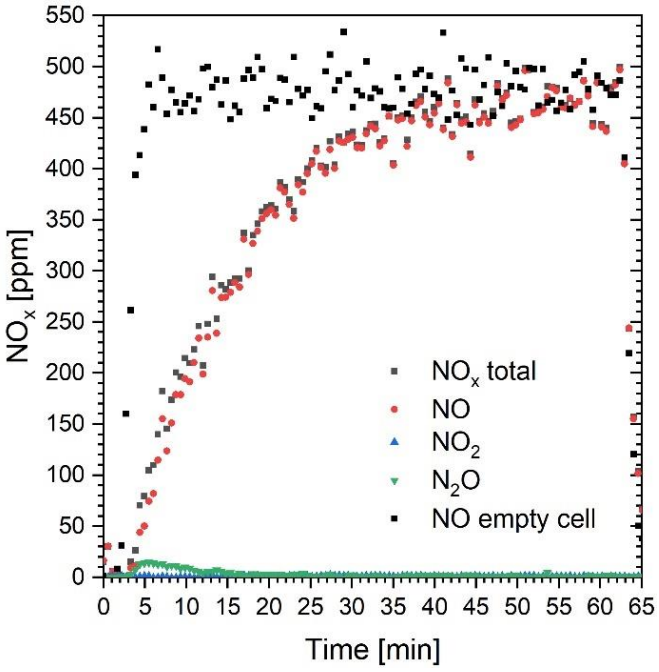

Fig. 5 NO_x breakthrough curves during NO_x storage at 30°C without oxygen in reductively pretreated Pt/CeO_2.

After oxidative pretreatment of the Pt/CeO_2 sample, finely dispersed PtO_x particles and metallic platinum was present on the ceria surface (see Table 1). During NO_x storage without oxygen only minor changes were observed for the F_{2g} position and Pt-O signal intensity (see Fig. S5). The NO_x storage capacity of oxidatively pretreated Pt/CeO_2 was determined as only 0.05 mmol/g, compared to 0.11 mmol/g for equally treated bare ceria (see Table 3). Therefore, it is obvious that deposited platinum occupied some of the NO adsorption sites. The consumption of Ce-O sites could not be captured by Raman spectroscopy in this case, since the signal-to-noise ratio was too low.

NO_x storage with oxygen in Pt/CeO_2

As described above, for bare ceria in the presence of oxygen, the NO_x storage mechanism is dominated by the formation of NO_2 and/or $[NO+O_2]$ complexes and therefore the consumption of surface oxygen Ce-O. In fact, on bare ceria, the NO_x storage capacity shows an exponential dependence on the consumption of surface oxygen (see Fig. 6). When platinum was loaded on ceria, the amount of surface oxygen decreased (see Table 2).

Even if a lower amount of surface oxygen was accessible for NO_x storage, the NO_x storage capacity of Pt loaded ceria was higher than expected compared to the consumed surface oxygen (see Fig. 6). Therefore, new reaction pathways must have opened up for NO_x storage.

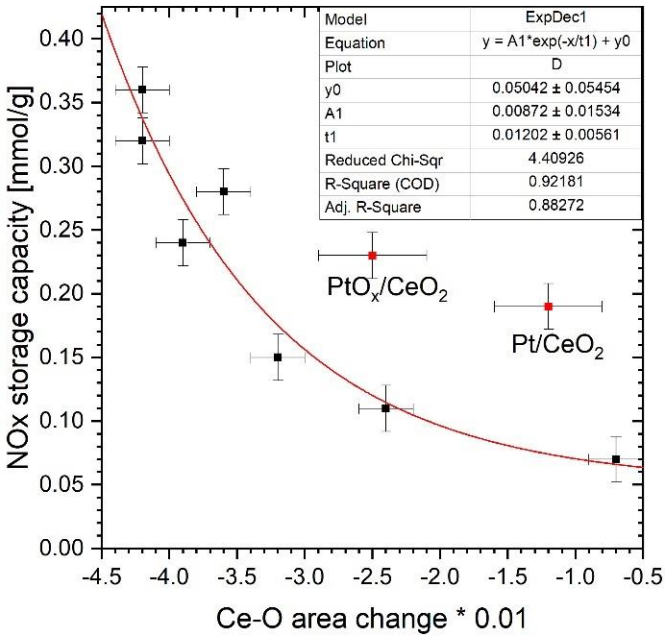

Fig. 6 NO_x storage capacity at 30°C as a function of the Raman Ce-O area change. Black squares correspond to bare ceria, while red squares correspond to oxidatively (PtO_x/CeO_2) and reductively pretreated (Pt/CeO_2) platinum loaded ceria.

As could be shown above for NO_x storage without oxygen in reductively pretreated Pt/CeO_2, metallic platinum can activate NO for reduction to N_2O and N_2 (see Fig. 5). However, no N_2O was observed during NO_x storage with oxygen (not shown). Thus, the higher NO_x storage capacity cannot be explained by NO activation on metallic platinum only; rather it is expected that also gas-phase oxygen was activated on platinum at 30°C, which can then be used for NO oxidation and restoration of NO adsorption sites. According to Li *et al.* room temperature oxygen activation on metallic platinum may lead to the formation of atomic oxygen, followed by spillover and migration on the ceria surface.[52] Since the higher NO_x storage capacity observed in our experiments cannot only be explained by the interface between platinum and ceria, NO_x storage in Pt/CeO_2 has to involve the migration of oxygen. Such a migration may proceed either by diffusion of atomic oxygen on the ceria surface or by healing of oxygen vacancies, including diffusion of oxygen vacancies further away towards metallic platinum due to the rising gradient.

For oxidatively pretreated Pt/CeO_2 a decrease in NO_x storage capacity was observed, as it was expected owing to the lower amount of surface oxygen compared to bare ceria (see Table 3). However, based on the consumption of surface oxygen being fully responsible for NO_x storage, the NO_x storage capacity was by 0.08 mmol/g higher than expected (see Fig. 6). Therefore, an additional pathway was accessible for NO_x storage in Pt/CeO_2. In Raman and UV-vis spectra a decrease in the Pt-O-Ce and PtO_x signal intensity was detected, indicating reduction and participation of PtO_x in NO_x storage (see Figs. 7 and S6). Consequently, NO_x was probably also stored at the interface of ceria and PtO_x.

As an estimate, on 1 g of Pt/CeO_2 there are around $9.6 \cdot 10^{-6}$ mol of platinum. Since the NO_x storage capacity was by 0.08 mmol/g higher than expected, and there was still some PtO_x on the sample after one hour of NO_x storage (see Fig. S6), the total amount of stored NO_x was still

too high to be explained by Ce-O sites and the PtO_x/CeO_2 interface only. Therefore, it is proposed that that PtO_x reduced to metallic platinum could activate gas-phase oxygen and NO.

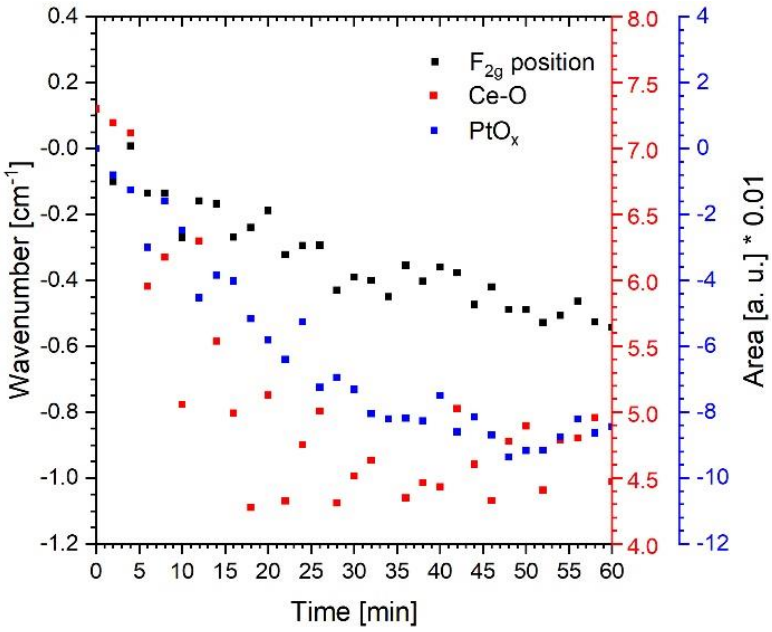

Fig. 7 Temporal behavior of the Raman F_{2g} position, Ce-O area, and PtO_x area during NO_x storage with oxygen in oxidatively pretreated Pt/CeO_2.

NO_x desorption

Under realistic conditions oxygen will always be present. Therefore, the role of platinum on the temperature-dependent NO_x desorption behavior in 20% O_2/N_2 was investigated after NO_x storage with oxygen in oxidatively and reductively pretreated Pt/CeO_2. For comparison the NO_x desorption behavior of oxidatively and reductively pretreated CeO_2 was also analyzed. The temperature-dependent NO_x desorption behavior is depicted in Fig. 8, demonstrating an influence of both the pretreatment and platinum loading. The percentage of stored NO_x released and the NO/NO_2 ratio

of desorbed NO_x at the respective temperature ranges is summarized in Table S2 for all samples studied.

Reductive pretreatment results in a higher amount of desorbed NO_x at low temperatures (see Fig. 8 and Table S2), indicating that NO was stored as a less stable NO_x species (e.g. nitrite). The predominant formation of nitrite species after reductive pretreatment has been shown previously for bare ceria.[12] However, during NO_x desorption of a reductively pretreated sample also NO_2 was observed, indicative of the presence of adsorbed nitrate species or oxidation of nitrite to nitrate with subsequent desorption or decomposition upon heating in oxygen. After NO_x storage in an oxidatively pretreated sample more NO_2 than NO was observed during NO_x desorption, strongly suggesting the formation of a larger fraction of nitrate during NO_x storage, consistent with the higher amount of desorbed NO_x in the temperature range 200-500°C (see Table S2) and in agreement with earlier results on NO_x storage with oxygen in oxidatively pretreated ceria.[12]

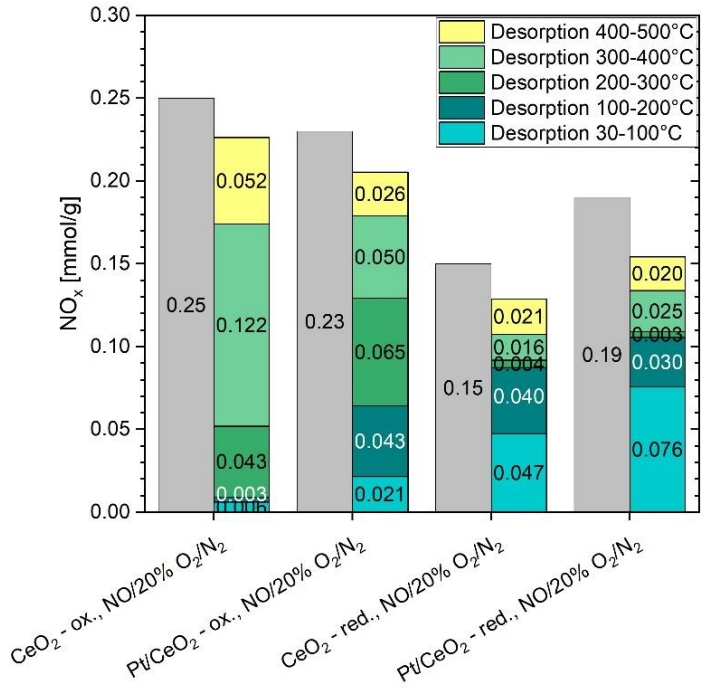

Fig. 8 NO_x storage capacities and temperature-dependent NO_x desorption behavior after one hour of NO_x storage at 30°C with oxygen and amount of desorbed NO_x in 20% O_2/N_2 for oxidatively and reductively pretreated CeO_2 and Pt/CeO_2.

For platinum-loaded ceria, differences in the temperature-dependent NO_x desorption behavior were observed for the two pretreatments. After oxidative pretreatment, more platinum was in an oxidized state (see Table 1, Figs. 2 and 3), resulting in more NO_x being desorbed within 30-300°C but less NO_x being desorbed within 300-500°C compared to bare ceria. On the other hand, reductive pretreatment of platinum-loaded ceria gives mainly rise to mainly metallic platinum (see Table 1 and Fig. 3), which compared to bare ceria leads to more NO_x being desorbed at low temperature (30-100°C), while the amount of desorbed NO_x within 100-200°C decreased and remained nearly the same at higher temperatures (200-500°C). Thus, variations in the platinum state resulted in significant differences in the NO_x storage and NO_x desorption behavior.

Using *in situ* Raman and UV-vis spectroscopy changes in the platinum state after each treatment can be monitored (see Fig. 9). Raman spectra are more suitable to detect the formation of PtO_x, since UV-vis spectra may be dominated by absorption within 400-1000 nm originating from larger metallic platinum particles (see Fig. 9d), masking the PtO_x signals. By contrast, in Raman spectra the formation of PtO_x is observed at temperatures >100°C for oxidatively and reductively pretreated Pt/CeO_2 (see Figs. 9a and b), whereas for reductively pretreated Pt/CeO_2 nearly no changes in UV-vis spectra were detected (see Fig. 9d). In contrast, for oxidatively pretreated Pt/CeO_2, UV-vis spectra are characterized by the PtO_x adsorption behavior. It is assumed that during NO_x storage in oxidatively pretreated Pt/CeO_2 finely dispersed and very small metallic platinum particles are formed, which had no influence on the UV-vis spectra shown here. On the other hand, upon NO_x storage, the absorption within 700-1000 nm and the PtO_x Raman signal intensity significantly dropped. Increasing the temperature, resulted in an overall increase of both the PtO_x signal and the 700-1000 nm absorption, strongly suggesting that PtO_x particles contributed to the absorption behavior within 700-1000 nm.

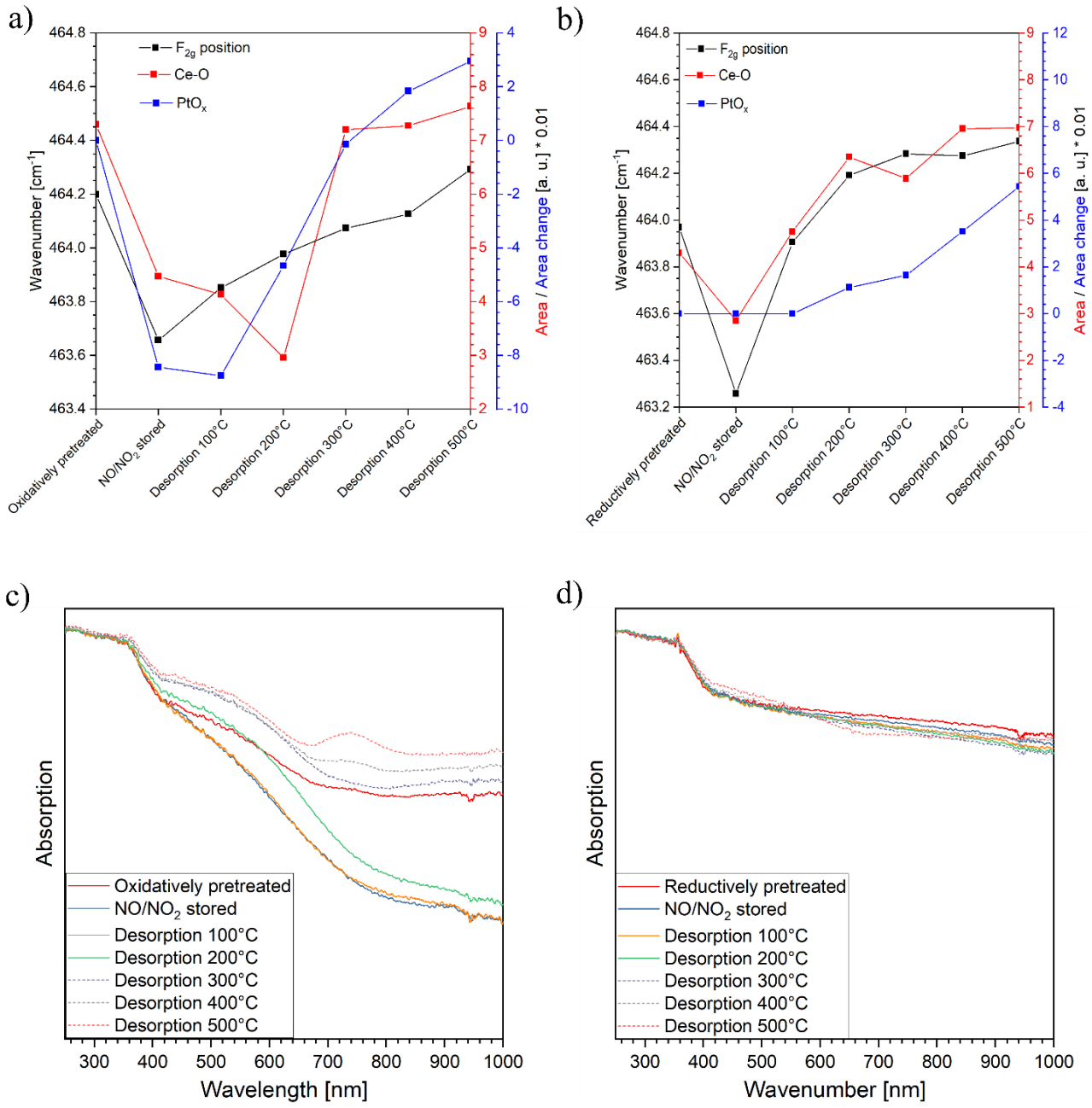

Fig. 9 Temperature-dependent evolution of the Raman F_{2g} position, Ce-O signal area, and PtO_x signal area change after NO_x storage in oxygen for a) oxidatively and b) reductively pretreated Pt/CeO_2. The corresponding UV-vis spectra are shown at the bottom for c) oxidatively and d) reductively pretreated Pt/CeO_2.

Closer inspection of the Raman spectral behavior of oxidatively pretreated Pt/CeO_2 reveals (see Fig. 9a) that, upon heating to 300°C, the PtO_x signal intensity returned approximately to its initial value after oxidative pretreatment. A similar observation was made in UV-vis spectra (see Fig. 9c), since the 500-1000 nm absorption after ramping to 300°C was only slightly higher than after oxidative pretreatment. At higher temperatures, both Raman and UV-Vis spectra show only smaller increases of the corresponding signals, whereas at 500°C an additional UV-Vis absorption band between 700 and 800 nm was detected. Without any further input (from theory) being available in the literature, we tentatively attribute the observed behavior of oxidatively pretreated Pt/CeO_2 to the presence of different PtO_x sites, leading to the observed shape and broadness of the UV-Vis absorption signals.

The oxidation of Pt^0 to PtO_x is dependent on the size of the metallic platinum particles.[23, 47] Since in our case the metallic platinum particles are small after oxidative pretreatment and subsequent NO_x storage, they are easily reoxidized at lower temperatures resulting in a higher amount of PtO_x, which can be observed by Raman and UV-vis spectroscopy (see Figs. 9a and c). For oxidatively pretreated Pt/CeO_2, most of the formed PtO_x reemerges at temperatures between 100 and 300°C; in this range also more NO_x was released as a result of the platinum loading (see Fig. 8 and Table S2). In the literature it was shown by isotopic experiments, that metallic platinum is preferentially reoxidized by lattice oxygen rather than gas-phase oxygen, while oxygen vacancies in the ceria lattice were oxidized by gas-phase oxygen.[41] From these observations it follows for oxidatively pretreated Pt/CeO_2 that upon heating metallic platinum is reoxidized by ceria lattice oxygen leading to a destabilization of adsorbed NO_x species and consequently a higher amount of desorbed NO_x within 30-300°C.

On the contrary, platinum particles on reductively pretreated Pt/CeO_2 are relatively large compared to the oxidatively pretreated sample. Hence, a significantly smaller amount of PtO_x formed within 100-300°C (see Fig. 9b), which had nearly no influence on the NO_x desorption in this temperature region. In UV-vis spectra PtO_x could only be detected upon desorption at 500°C (see Fig. 9d).

Discussion

NO_x storage

Different factors have an influence on the NO_x adsorption and desorption behavior. In this work we elaborated the influence of platinum, pretreatment, and gas-phase oxygen, by investigating the NO_x storage and desorption of oxidatively and reductively pretreated ceria and platinum-loaded ceria. The pretreatment had an influence on the properties of ceria and platinum and therefore on the NO_x storage and desorption behavior.

After oxidative pretreatment of bare ceria, the NO_x storage behavior was strongly dependent on the presence and concentration of gas-phase oxygen, fully consistent with literature findings on ceria[12, 35, 37, 38] and other NO_x storage components as $BaCO_3$.[69] In the absence of oxygen, the NO_x storage capacity was significantly lower (see Table 3) and nearly no contribution of ceria (sub)surface oxygen was observed, indicating no or only weak interactions of NO with surface oxygen. These findings are in good agreement with previous literature results, which have proposed a stronger adsorption of NO on oxygen vacancies.[66-68] However, as the observed NO_x storage capacity cannot be explained by oxygen vacancy sites only, besides oxygen vacancies also other NO adsorption sites such as ceria edges may play a role in NO_x storage.[35]

Reductive pretreatment of ceria at 400°C in hydrogen resulted in a surface reduction, consistent with the results of Laachir *et al.*.[70] As NO interacts more strongly with surface oxygen vacancies,[66-68] we expect NO adsorption on such sites, giving rise to nitrite formation. For bare ceria, no decomposition of NO to N_2 at low temperatures was reported.[2] Therefore, it is proposed that after NO adsorption on oxygen vacancies and formation of nitrite species, migration of nitrite is kinetically hindered. All in all, reductively pretreated ceria shows the lowest NO_x storage capacity (see Table 3 and Fig. 4). The relatively high NO_x storage capacity for oxidatively pretreated ceria after NO_x storage without oxygen can be explained by residual adsorbed oxygen, having a strong influence on the NO_x storage mechanism.

In the presence of gas-phase oxygen, NO is partly oxidized to NO_2 as a consequence of the thermodynamic equilibrium (see Fig. S3). In addition, a significantly higher NO_x storage capacity was observed, accompanied by a significant decrease of ceria Ce-O surface and subsurface oxygen (F_{2g} redshift) (see Table 3). Since nearly no decrease of (sub)surface oxygen was detected during NO_x storage without oxygen, it stands to reason that NO was not able to react with surface oxygen. By contrast, in the presence of oxygen, NO_2 was formed and could adsorb on surface oxygen sites leading to a decrease of Ce-O sites. However, the increase in NO_x storage capacity cannot be explained only by the adsorption of NO_2, since only one fifth of the amount of NO was oxidized to NO_2, while the NO_x storage capacity had more than doubled. Consequently, it is proposed that [$NO+O_2$] complexes are formed, possibly involving prior activation of molecular oxygen on ceria, which in turn could react with ceria lattice oxygen. A reaction of NO with O_2 leading to [$NO+O_2$] formation, as e.g. peroxynitrite, has been discussed previously for other systems.[65, 71] As reported for a copper complex, O_2 can be adsorbed as superoxide, reacting with NO to form peroxynitrite.[30]

A similar mechanism is conceivable for ceria, in particular, as formation of superoxides on ceria was already evidenced in previous studies.[10, 56, 57, 72]

In the presence of oxygen, the direct adsorption of NO on oxygen vacancies was suppressed and the NO_x storage mechanism was dominated by the reaction of NO_2 and/or [$NO+O_2$] complexes with surface oxygen sites, since a correlation between surface oxygen decrease and NO_x storage capacity was observed (see Fig. 6). As oxidatively pretreated ceria had a significantly higher amount of surface oxygen sites, the NO_x storage capacity for oxidatively pretreated ceria was higher than for reductively pretreated ceria.

In the next step, the influence of Pt on the NO_x storage behavior was investigated. After reductive pretreatment, platinum was present almost exclusively as Pt^0 (see Table 1 and Fig. 3). Besides, ceria was reduced more strongly on the (sub)surface compared to bare ceria, caused by hydrogen spillover (see Table 2), in accordance with previous studies.[1, 41, 73] Upon NO exposure without oxygen, in the initial 15 min the formation of N_2O was observed by IR gas-phase analysis (see Fig. 5), indicating a reduction of NO to N_2O and N_2.[2] It is expected, that the oxygen atom of NO is used to heal the oxygen vacancies on ceria.[1, 2] As the NO decrease during NO exposure was too high to be explained only by NO reduction, NO was partly reduced on the surface, but also stored. Compared to bare ceria, the NO_x storage capacity of Pt/CeO_2 was nearly three times higher (see Fig. 4 and Table 3), indicating the supportive effect of Pt for NO storage without oxygen. One may expect, that during NO reduction also activated oxygen was formed on the ceria surface with the aid of Pt, which could undergo reaction with NO to NO_2 or [$NO+O_2$] complexes, followed by reaction with ceria lattice oxygen. Such a scenario is strongly supported by the observed decrease in Ce-O area and the F_{2g} redshift (see Table 3).

When oxygen was present during NO_x storage in reductively pretreated Pt/CeO_2, no N_2O formation was observed in the gas-phase IR spectra. Therefore, either no reduction of NO had occurred or the concentration of N_2O was too low to be detected. For bare ceria, a clear correlation between Ce-O consumption and NO_x storage capacity was found (see Fig. 6). On reductively pretreated Pt/CeO_2, the surface oxygen concentration on ceria was the lowest and compared to the Ce-O consumption, the NO_x storage capacity was too high to be explained by Ce-O consumption only (see Fig. 6). Therefore, metallic platinum supported the NO_x storage in ceria, e.g. by activating gas-phase oxygen at 30°C, leading to a reoxidation of the ceria surface. This in turn could explain the lower overall Ce-O consumption compared to the high NO_x storage capacity. An activation of gas-phase oxygen by Pt/CeO_2 was already discussed by Li *et al.*.[52] As the amount of additionally stored NO_x was too high to be explained by Pt^0/CeO_2 interface sites only, oxygen migration from the interface must have occurred. Such migration may take place either via diffusion of activated oxygen species over the ceria surface to an oxygen vacancy followed by vacancy healing or by healing of oxygen vacancies in the proximity of metallic platinum particles and subsequent diffusion of oxygen vacancies towards the platinum/ceria interface. To this end, Chen *et al.* showed by DFT calculations that on defect-rich ceria oxygen ions can diffuse over the ceria surface without an energy barrier, while the energy barrier increased to 1.58 eV on a perfect ceria surface. In comparison, the migration of oxygen vacancies was associated with an energy barrier of 0.48 to 0.87 eV, depending on the oxygen-vacancy concentration.[74] A similar value for the migration of oxygen vacancies of 0.53 eV was reported by Nolan *et al.*.[75] Therefore, it is assumed, that oxygen vacancies farer away from the Pt particles were healed via migration of oxygen ions over a defective ceria surface rather than migration of oxygen vacancies to the Pt/ceria interface.

When the Pt/CeO_2 sample was pretreated oxidatively, more PtO_x than Pt^0 was found on the surface (see Table 1). Furthermore, in the absence of oxygen during NO_x storage, the NO_x storage capacity was lower for oxidatively pretreated Pt/CeO_2 than for bare ceria (see Fig. 4 and Table 3). IR gas-phase analysis detected no N_2O, indicating that metallic platinum with a certain particle size is needed for NO reduction. As for bare ceria, nearly no F_{2g} shift was observed, indicating that NO was not able to react with ceria surface oxygen. Therefore, Pt showed no beneficial effect for NO_x storage. The lower NO_x storage capacity of oxidatively pretreated Pt/CeO_2 can be explained by the occupation of NO adsorption sites by PtO_x or metallic platinum. Zhou *et al.* showed by using STM, that metallic platinum particles preferentially interacted with oxygen vacancies.[76] If oxygen vacancies are occupied by platinum, NO cannot adsorb on these sites resulting in an decrease of NO_x storage capacity.

In contrast, in the presence of oxygen, NO_x storage was supported by Pt. Again, the Ce-O consumption was too low to explain the high NO_x storage capacity (see Fig. 6). Using Raman spectroscopy, it was observed that the Pt-O signal intensity decreased (see Fig. 7), indicating a participation of PtO_x in NO_x storage. However, it should be noted, that no decrease of the PtO_x signal intensity in Raman spectra was observed, when NO was stored without oxygen (see Fig. S5). Therefore, NO itself could not interact with PtO_x. Again, NO_2 or $[NO+O_2]$ complexes are needed for the interaction with PtO_x. Nevertheless, the NO_x storage was still too high to be explained only by the participation of PtO_x in NO_x storage, since the amount of deposited Pt was too low. On the other hand, activation of gas-phase oxygen is expected to play a role also over oxidatively pretreated Pt/CeO_2, either via already existing Pt^0 particles (see Table 1) or by metallic platinum particles formed during the interaction of NO_2 or $[NO+O_2]$ with PtO_x. Oxygen activation

may result in the reoxidation of surface oxygen vacancies, explaining the higher NO_x storage capacity compared to the consumed ceria surface oxygen.

NO_x desorption

Based on the influence of the pretreatment and the state of platinum on NO_x storage, also an influence on the NO_x desorption is expected. To this end, the most important factor is the type of species responsible for NO_x storage, i.e., nitrite or nitrate. Oxidative pretreatment leads to more nitrate formation and consequently a larger fraction of NO_x desorbing at higher temperatures. In our previous studies it has been shown, that primarily nitrites were formed, which in turn were transformed to nitrates at long storage times.[12] A conversion of nitrites to nitrates during NO_x storage in the presence of gas-phase oxygen was also observed at higher temperatures (>200°C).[7, 35, 37, 38] If samples were pretreated oxidatively and NO was stored in the presence of oxygen for one hour at 30°C, around 60-87% of the stored NO_x were released at 200-500°C, while more NO_2 than NO was observed in the outlet confirming the formation of stable nitrates (see Table S2). By contrast, reductive pretreatment led mainly to the formation of nitrites[12] and therefore 55-58% of the stored NO_x were already released at 30-200°C, while in the outlet more NO than NO_2 was observed (see Table S2).

If ceria was loaded with Pt, the amount of NO_x desorbing at low temperatures significantly increased, while compared to bare ceria, the overall amount of desorbed NO_x decreased. Since room-temperature NO reduction over Pt/CeO_2 was already reported[2] and is consistent with our findings, the decrease in the overall amount of desorbed NO_x can be explained by NO reduction occurring concurrently with NO_x adsorption.

NO_x desorption itself was also dependent on the Pt state. Metallic platinum led mainly to a higher fraction of NO_x desorbing within 30-100°C, while less NO_x desorbed between 100 and 300°C, and the NO/NO_2 ratio remained nearly unchanged between 30 and 200°C compared to bare ceria (see Table S2). On Pt-loaded ceria, within the region 200-300°C, only NO_2 was observed during desorption, whereas on bare ceria also NO was detected. The change in NO/NO_2 ratio can be explained by NO oxidation to NO_2 following NO_x desorption, consistent with the literature, showing that Pt-loaded ceria can oxidize NO at temperatures >200°C.[23]

The higher amount of desorbed NO_x within 30-100°C over reductively pretreated Pt/CeO_2 can be explained by a destabilization of NO_x adsorption sites in the proximity of metallic platinum. In DFT calculations, a charge transfer from metallic platinum to the ceria surface was observed,[77-79] which is expected to result in a weakening of adsorbed NO_x, since for NO_x adsorption also electrons are transferred from the NO_x molecule to the ceria surface.

If Pt-loaded ceria is pretreated oxidatively, PtO_x formation is observed. Upon NO exposure the PtO_x is partly reduced to metallic platinum. However, during NO_x desorption, reoxidation of formed metallic platinum particles to PtO_x occurred, particularly, in the temperature region 100-300°C (see Fig. 9). At these temperatures also the largest increase of desorbed NO_x for oxidatively pretreated Pt/CeO_2 was observed compared to bare ceria (see Table S2), suggesting that the reoxidation of metallic platinum induced a destabilization of adsorbed NO_x species. In the literature it was found by isotopic experiments, that the reoxidation of metallic platinum on ceria proceeded with the aid of ceria lattice oxygen rather than gas-phase oxygen.[41] If oxygen is eliminated from the ceria lattice because of the formation of PtO_x, the ceria will be reduced leading in turn to a destabilization of adsorbed NO_x species.

Conclusions

In this contribution, the role of platinum on the NO_x storage and desorption behavior in ceria at 30°C was investigated. The investigations were performed by online FT-IR gas-phase analysis, in combination with *in situ* Raman and UV-vis spectroscopy. The combination of Raman and UV-vis spectroscopy gave information on the state of platinum on ceria. While Raman spectra provided access to finely dispersed PtO_x, UV-vis spectra allowed detection of larger metallic platinum particles by broad absorption within 400-1000 nm. However, very finely dispersed platinum particles on ceria showed no absorption in this region and therefore could probably not be detected by UV-vis spectroscopy. With the aid of online FT-IR gas-phase analysis the amount of adsorbed and released NO_x was detected, providing quantitative information on the NO_x storage capacity.

During NO_x storage and desorption, Raman spectroscopy provided the opportunity to analyze changes in ceria surface and subsurface oxygen, as well as PtO_x during NO_x storage. Most notably, no reaction of NO with (sub)surface oxygen and PtO_x was observed in the absence of oxygen. Only in the presence of gas-phase oxygen a decrease in the amount of (sub)surface oxygen and PtO_x was detected, indicating reaction and storage of NO_x. Therefore, it is assumed that only NO_2 and $[NO+O_2]$ complexes are able to react with surface oxygen and finely dispersed PtO_x, leading to new reaction pathways for NO_x storage. It should be noted that in the presence of oxygen, the NO_x storage behavior was dominated by oxygen-mediated reaction pathways determining the NO_x storage capacity.

As expected, the state of platinum on ceria was dependent on the pretreatment of the sample. Oxidative pretreatment led to the formation of finely dispersed PtO_x, while reductive pretreatment resulted in metallic platinum particles. By detailed analysis of the NO_x storage behavior, we could show that both platinum states participated in the NO_x storage at 30°C and

each platinum state led to new reaction pathways. However, upon deposition of platinum on ceria, NO_x adsorption sites are occupied leading to a concurrent effect between the decrease of NO_x adsorption sites and new reaction pathways for NO_x storage.

For metallic platinum on ceria we propose a room-temperature activation of gas-phase oxygen, leading to a healing of oxygen vacancies on the ceria surface and consequently the formation of new NO_x adsorption sites. By contrast, in the absence of oxygen, a reduction of NO by metallic platinum to N_2O and N_2 was detected. All in all, after reductive pretreatment the platinum-loaded ceria showed a better performance in NO_x storage than bare ceria. For oxidatively pretreated Pt/CeO_2 the loss of NO_x adsorption sites, caused by platinum deposition and subsequent formation of PtO_x, overmatched the supportive effect of the formed PtO_x in NO_x storage. Nevertheless, the participation and supportive effect of PtO_x in NO_x storage was shown.

The NO_x desorption behavior was on one hand dependent on the pretreatment and on the other hand on the presence of platinum. Oxidative pretreatment resulted in the formation of a higher fraction of nitrates and therefore the highest amount of NO_x desorbed within 200-500°C. By contrast, after reductive pretreatment more nitrite was formed, thus 55-58% of the stored NO_x was released already between 30 and 200°C. The deposition of platinum on ceria led to a larger amount of NO_x desorbing at temperatures <300°C. If mainly larger metallic platinum particles were present, especially the amount of NO_x desorbing below 100°C increased. By contrast, if finely dispersed metallic platinum particles were formed during NO_x storage, the amount of NO_x desorbing within 30-300°C increased, while the largest amount was desorbed within 100-300°C. The overall increase in desorbed NO_x within 100-300°C was associated with the reoxidation of small Pt^0 particles to PtO_x.

Considering all results, oxidatively pretreated ceria showed the best performance in NO_x storage at 30°C and in the NO_x desorption behavior, leading to the largest NO_x storage capacity and largest amounts of desorbed NO_x within 200-500°C.

Conflicts of interest

There are no conflicts to declare.

Acknowledgments

The authors thank Kathrin Hofmann for XRD measurements, Silvio Heinschke for N_2 adsorption/desorption measurements, and Karl Kopp for XPS analysis as well as technical support. This work was supported by the Deutsche Forschungsgemeinschaft (DFG, HE 4515/3-2). A.F. thanks Haldor Topsøe for the possibility to do some of the initial experiments of this project at their site.

References

1. Y. Wang, R. Oord, D. van den Berg, B. M. Weckhuysen and M. Makkee, *Chemcatchem*, 2017, **9**, 2935-2938.
2. M. Haneda, Y. Kintaichi and H. Hamada, *Phys. Chem. Chem. Phys.*, 2002, **4**, 3146-3151.

3. M. V. Twigg, *Johnson Matthey Technology Review*, 2015, **59**, 221-232.
4. G. Guo, D. Dobson, J. Warner, W. Ruona and C. K. Lambert, *SAE International*, 2012, 2012-2001-0371.
5. T. V. Johnson, *SAE Int. J. Engines*, 2015, **8**, 1152-1166.
6. Y. Zhang, Y. B. Yu and H. He, *Catal. Sci. Technol.*, 2016, **6**, 3950-3962.
7. V. Rico-Perez, A. Bueno-Lopez, D. J. Kim, Y. Y. Ji and M. Crocker, *Appl. Catal., B*, 2015, **163**, 313-322.
8. L. Wang, R. Ran, X. D. Wu, M. Li and D. Weng, *J. Rare Earth*, 2013, **31**, 1074-1080.
9. T. Wang, L. W. Jia, X. T. Wang, G. Wang, F. Q. Luo and J. M. Wang, *Rare Metals*, 2019, **38**, 81-86.
10. A. Filtschew, D. Stranz and C. Hess, *Phys. Chem. Chem. Phys.*, 2013, **15**, 9066-9069.
11. C. A. Shi, Y. Y. Ji, U. M. Graham, G. Jacobs, M. Crocker, Z. S. Zhang, Y. Wang and T. J. Toops, *Appl. Catal., B*, 2012, **119**, 183-196.
12. A. Filtschew and C. Hess, *Appl. Catal., B*, 2018, **237**, 1066-1081.
13. J. R. Theis, *Catal. Today*, 2016, **267**, 93-109.
14. J. R. Theis and C. K. Lambert, *Catal. Today*, 2015, **258**, 367-377.
15. J. R. Theis and C. K. Lambert, *Catal. Today*, 2019, **320**, 181-195.
16. Y. T. Gu and W. S. Epling, *Appl Catal a-Gen*, 2019, **570**, 1-14.
17. T. J. Toops, D. B. Smith and W. P. Partridge, *Catal. Today*, 2006, **114**, 112-124.
18. T. J. Toops, D. B. Smith and W. P. Partridge, *Appl. Catal., B*, 2005, **58**, 245-254.
19. C. Hess and J. H. Lunsford, *J. Phys. Chem. B*, 2003, **107**, 1982-1987.
20. C. Hess and J. H. Lunsford, *J. Phys. Chem. B*, 2002, **106**, 6358-6360.
21. S. Jones, Y. Y. Ji and M. Crocker, *Catal. Lett.*, 2016, **146**, 909-917.
22. Y. Y. Ji, T. J. Toops and M. Crocker, *Catal. Lett.*, 2007, **119**, 257-264.
23. J. Y. Luo, W. S. Epling, G. S. Qi and W. Li, *Catal. Lett.*, 2012, **142**, 946-958.
24. I. Atribak, B. Azambre, A. B. Lopez and A. Garcia-Garcia, *Appl. Catal., B*, 2009, **92**, 126-137.
25. B. Azambre, I. Atribak, A. Bueno-Lopez and A. Garcia-Garcia, *J. Phys. Chem. C*, 2010, **114**, 13300-13312.
26. B. Azambre, L. Zenboury, F. Delacroix and J. V. Weber, *Catal. Today*, 2008, **137**, 278-282.
27. S. S. Chaugule, V. F. Kispersky, J. L. Ratts, A. Yezerets, N. W. Currier, F. H. Ribeiro and W. N. Delgass, *Appl. Catal., B*, 2011, **107**, 26-33.
28. J. H. Kwak, D. H. Kim, T. Szailer, C. H. F. Peden and J. Szanyi, *Catal. Lett.*, 2006, **111**, 119-126.
29. Y. Y. Ji, T. J. Toops, J. A. Pihl and M. Crocker, *Appl. Catal., B*, 2009, **91**, 329-338.
30. L. F. Lv, X. Q. Wang, M. Q. Shen, Q. Q. Zhang and J. Wang, *Chem. Eng. J.*, 2013, **222**, 401-410.
31. X. Q. Wang, L. F. Lv, Q. Q. Zhang, Y. W. Zhang, J. Wang and M. Q. Shen, *Catal. Sci. Technol.*, 2013, **3**, 200-207.
32. Y. Y. Ji, D. Y. Xu, S. L. Bai, U. Graham, M. Crocker, B. B. Chen, C. Shi, D. Harris, D. Scapens and J. Darab, *Ind. Eng. Chem. Res.*, 2017, **56**, 111-125.
33. A. Y. Stakheev, I. S. Mashkovsky, G. O. Bragina, G. N. Baeva, N. S. Telegina, K. M. Larsen, A. L. Kustov and J. R. Thogersen, *Top. Catal.*, 2016, **59**, 931-937.
34. M. Y. Mihaylov, E. Z. Ivanova, H. A. Aleksandrov, P. S. Petkov, G. N. Vayssilov and K. I. Hadjiivanov, *Chem. Commun.*, 2015, **51**, 5668-5671.

35. M. Y. Mihaylov, E. Z. Ivanova, H. A. Aleksandrov, P. S. Petkov, G. N. Vayssilov and K. I. Hadjiivanov, *Mol. Catal.*, 2018, **451**, 114-124.
36. M. Y. Mihaylov, E. Z. Ivanova, H. A. Aleksandrov, P. St Petkov, G. N. Vayssilov and K. I. Hadjiivanov, *Appl. Catal. B*, 2015, **176**, 107-119.
37. S. Philipp, A. Drochner, J. Kunert, H. Vogel, J. Theis and E. S. Lox, *Top. Catal.*, 2004, **30-1**, 235-238.
38. M. O. Symalla, A. Drochner, H. Vogel, S. Philipp, U. Gobel and W. Muller, *Top. Catal.*, 2007, **42-43**, 199-202.
39. L. L. Murrell, S. J. Tauster, D. R. Anderson, F. Bozonverduraz, S. I. Woo, W. C. Conner, J. C. Conesa, D. G. Blackmond, M. Ichikawa and C. H. Bartholomew, *Stud. Surf. Sci. Catal.*, 1993, **75**, 681-690.
40. M. S. Brogan, T. J. Dines and J. A. Cairns, *J. Chem. Soc., Faraday Trans.*, 1994, **90**, 1461-1466.
41. W. Y. Lin, A. A. Herzing, C. J. Kiely and I. E. Wachs, *J. Phys. Chem. C*, 2008, **112**, 5942-5951.
42. J. Choi, H. Park and M. R. Hoffmann, *J. Phys. Chem. C*, 2010, **114**, 783-792.
43. Z. Xiong, H. Wang, N. Xu, H. Li, B. Fang, Y. Zhao, J. Zhang and C. Zheng, *Int. J. Hydrogen Energ*, 2015, **40**, 10049-10062.
44. A. V. Vorontsov, E. N. Savinov and J. Zhensheng, *J. Photochem. Photobiol. A,* 1999, **125**, 113-117.
45. Y. Hu, X. Song, S. M. Jiang and C. H. Wei, *Chem. Eng. J.*, 2015, **274**, 102-112.
46. A. Naitabdi, R. Fagiewicz, A. Boucly, G. Olivieri, F. Bournel, H. Tissot, Y. W. Xu, R. Benbalagh, M. G. Silly, F. Sirotti, J. J. Gallet and F. Rochet, *Top. Catal.*, 2016, **59**, 550-563.
47. A. M. Ganzler, M. Casapu, P. Vernoux, S. Loridant, F. J. C. S. Aires, T. Epicier, B. Betz, R. Hoyer and J. D. Grunwaldt, *Angew. Chem. Int. Ed.*, 2017, **56**, 13078-13082.
48. Y. Nagai, K. Dohmae, Y. Ikeda, N. Takagi, T. Tanabe, N. Hara, G. Guilera, S. Pascarelli, M. A. Newton, O. Kuno, H. Y. Jiang, H. Shinjoh and S. Matsumoto, *Angew. Chem. Int. Ed.*, 2008, **47**, 9303-9306.
49. J. D. Grunwaldt and A. Baiker, *Phys. Chem. Chem. Phys.*, 2005, **7**, 3526-3539.
50. G. W. Graham, W. H. Weber, J. R. Mcbride and C. R. Peters, *J. Raman Spectrosc.*, 1991, **22**, 1-9.
51. Y. Y. Ji, T. J. Toops, U. M. Graham, G. Jacobs and M. Crocker, *Catal. Lett.*, 2006, **110**, 29-37.
52. C. Li, Y. Z. Song, Y. X. Chen, Q. Xin, X. W. Han and W. Z. Li, *Spillover and Migration of Surface Species on Catalysts*, 1997, **112**, 439-446.
53. P. Beato, E. Schachtl, K. Barbera, F. Bonino and S. Bordiga, *Catal. Today*, 2013, **205**, 128-133.
54. C. Schilling, A. Hofmann, C. Hess and M. V. Ganduglia-Pirovano, *J. Phys. Chem. C*, 2017, **121**, 20834-20849.
55. W. H. Weber, K. C. Hass and J. R. Mcbride, *Phys. Rev. B*, 1993, **48**, 178-185.
56. V. V. Pushkarev, V. I. Kovalchuk and J. L. d'Itri, *J. Phys. Chem. B*, 2004, **108**, 5341-5348.
57. Z. Wu, M. Li, J. Howe, H. M. Meyer and S. H. Overbury, *Langmuir*, 2010, **26**, 16595-16606.
58. M. Daniel and S. Loridant, *J. Raman Spectrosc.*, 2012, **43**, 1312-1319.

59. Y. Nagai, T. Hirabayashi, K. Dohmae, N. Takagi, T. Minami, H. Shinjoh and S. Matsumoto, *J. Catal.*, 2006, **242**, 103-109.
60. Z. Say, E. I. Vovk, V. I. Bukhtiyarov and E. Ozensoy, *Appl. Catal. B*, 2013, **142**, 89-100.
61. S. Alayoglu, K. J. An, G. Melaet, S. Y. Chen, F. Bernardi, L. W. Wang, A. E. Lindeman, N. Musselwhite, J. H. Guo, Z. Liu, M. A. Marcus and G. A. Somorjai, *J. Phys. Chem. C*, 2013, **117**, 26608-26616.
62. C. W. M. Castleton, J. Kullgren and K. Hermansson, *J. Chem. Phys.*, 2007, **127**.
63. G. R. Rao and H. R. Sahu, *Proc. Indian Acad. Sci. Chem. Sci.*, 2001, **113**, 651-658.
64. C. Binet, A. Badri and J. C. Lavalley, *J. Phys. Chem.*, 1994, **98**, 6392-6398.
65. H. Tsukahara, T. Ishida and M. Mayumi, *Nitric Oxide Biol. Chem.*, 1999, **3**, 191-198.
66. M. Nolan, *J. Phys. Chem. C*, 2009, **113**, 2425-2432.
67. Z. X. Yang, T. K. Woo and K. Hermansson, *Surf. Sci.*, 2006, **600**, 4953-4960.
68. J. Zhang, X. Q. Gong and G. Z. Lu, *Phys. Chem. Chem. Phys.*, 2014, **16**, 16904-16908.
69. T. C. Watling, P. D. Bolton and D. Swallow, *Chem. Eng. Sci.*, 2018, **178**, 312-323.
70. A. Laachir, V. Perrichon, A. Badri, J. Lamotte, E. Catherine, J. C. Lavalley, J. Elfallah, L. Hilaire, F. Lenormand, E. Quemere, G. N. Sauvion and O. Touret, *J. Chem. Soc., Faraday Trans.*, 1991, **87**, 1601-1609.
71. D. Maiti, D. H. Lee, A. A. N. Sarjeant, M. Y. M. Pau, E. I. Solomon, K. Gaoutchenova, J. Sundermeyer and K. D. Karlin, *J. Am. Chem. Soc.*, 2008, **130**, 6700-+.
72. Y. Zhao, B. T. Teng, X. D. Wen, Y. Zhao, Q. P. Chen, L. H. Zhao and M. F. Luo, *J. Phys. Chem. C*, 2012, **116**, 15986-15991.
73. A. M. Ganzler, M. Casapu, F. Maurer, H. Stormer, D. Gerthsen, G. Ferre, P. Vernaux, B. Bornmann, R. Frahm, V. Murzin, M. Nachtegaal, M. Votsmeier and J. D. Grunwaldt, *ACS Catal.*, 2018, **8**, 4800-4811.
74. H. T. Chen, J. G. Chang, H. L. Chen and S. P. Ju, *J. Comp. Chem.*, 2009, **30**, 2433-2442.
75. M. Nolan, J. E. Fearon and G. W. Watson, *Solid State Ionics*, 2006, **177**, 3069-3074.
76. Y. H. Zhou, J. M. Perket and J. Zhou, *J. Phys. Chem. C*, 2010, **114**, 11853-11860.
77. P. Tereshchuk, R. L. H. Freire, C. G. Ungureanu, Y. Seminovski, A. Kiejna and J. L. F. Da Silva, *Phys. Chem. Chem. Phys.*, 2015, **17**, 13520-13530.
78. T. Q. Nguyen, M. C. S. Escano, H. Nakanishi, H. Kasai, H. Maekawa, K. Osumi and K. Sato, *Appl. Surf. Sci.*, 2014, **288**, 244-250.
79. S. M. Kozlov and K. M. Neyman, *J. Catal.*, 2016, **344**, 507-514.

TOC entry

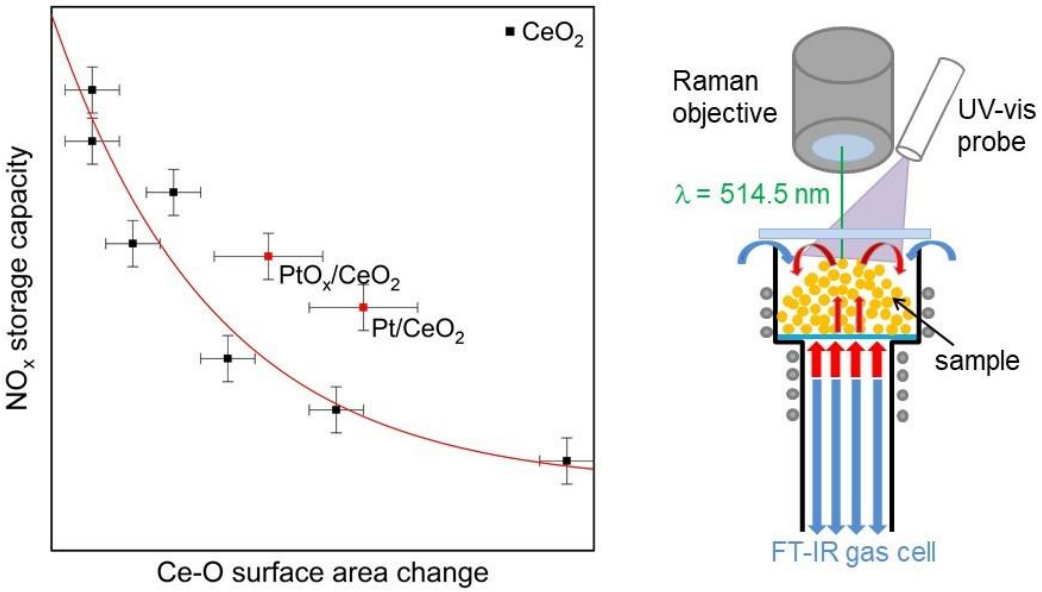

Elucidating the role of platinum on NO_x storage / desorption of ceria by online gas-phase analysis combined with *in situ* spectroscopy.